Earth and Planetary Science Letters 396 (2014) 179–189

Contents lists available at ScienceDirect

Earth and Planetary Science Letters

www.elsevier.com/locate/epsl

Constraints on the formation age and evolution of the Moon from ^{142}Nd–^{143}Nd systematics of Apollo 12 basalts

Claire L. McLeod *, Alan D. Brandon, Rosalind M.G. Armytage

Department of Earth and Atmospheric Sciences, Science and Research 1, University of Houston, 4800 Calhoun Road, Houston, TX, 77204-5007, USA

ARTICLE INFO

Article history:
Received 7 February 2014
Received in revised form 3 April 2014
Accepted 4 April 2014
Available online 3 May 2014
Editor: T.M. Harrison

Keywords:
lunar mantle
Apollo mare basalts
^{142}Nd
magma ocean
lunar evolution

ABSTRACT

The Moon likely formed as a result of a giant impact between proto-Earth and another large body. The timing of this event and the subsequent lunar differentiation timescales are actively debated. New high-precision Nd isotope data of Apollo mare basalts are used to evaluate the Low-Ti, High-Ti and KREEP mantle source reservoirs within the context of lunar formation and evolution. The resulting models are assessed using both reported ^{146}Sm half-lives (68 and 103 Myr). The linear relationship defined by ^{142}Nd–^{143}Nd systematics does not represent multi-component mixing and is interpreted as an isochron recording a mantle closure age for the Sm–Nd system in the Moon. Using a chondritic source model with present day μ ^{142}Nd of −7.3, the mare basalt mantle source reservoirs closed at 4.45^{+10}_{-09} Ga ($t_{1/2}$ $^{146}Sm = 68$ Myr) or 4.39^{+16}_{-14} Ga ($t_{1/2}$ $^{146}Sm = 103$ Myr). In a superchondritic, 2-stage evolution model with present day $\mu^{142}Nd$ of 0, mantle source closure ages are constrained to 4.41^{+10}_{-08} ($t_{1/2}$ $^{146}Sm = 68$ Myr) or 4.34^{+15}_{-14} Ga ($t_{1/2}$ $^{146}Sm = 103$ Myr).

The lunar mantle source reservoir closure ages <4.5 Ga may be reconciled by 3 potential scenarios. First, the Moon formed later than currently favored models indicate, such that the lunar mantle closure age is near or at the time of lunar formation. Second, the Moon formed *ca.* 4.55 to 4.47 Ga and small amounts of residual melts were sustained within a crystallizing lunar magma ocean (LMO) for up to *ca.* 200 Myr from tidal heating or asymmetric LMO evolution. Third, the LMO crystallized rapidly after early Moon formation. Thus the Sm–Nd mantle closure age represents a later resetting of isotope systematics. This may have resulted from a global wide remelting event. While current Earth-Moon formation constraints cannot exclusively advocate or dismiss any of these models, the fact that U–Pb ages and Hf isotopes for Jack Hills zircons from Australia are best explained by an Earth that re-equilibrated at 4.4 Ga or earlier following the Moon-forming impact, does not favor a later forming Moon. If magma oceans crystallize in a few million years as currently advocated, then a global resetting, possibly by a large impact at 4.40 to 4.34 Ga, such as that which formed the South Pole Aitken Basin, best explains the late mantle closure age for the coupled Sm–Nd isotope systematics presented here.

1. Introduction

Four decades after the return of the Apollo lunar samples, the formation age of the Moon and its early evolution remain elusive. The idea that the Moon differentiated within several 100 million years of solar system formation is derived from the observation that the positive Eu anomalies of the ancient lunar highland anorthosites complement the positive Eu anomalies of the younger lunar mare basalts (Taylor, 1973; Taylor and Jakes, 1974; Carlson and Lugmair, 1981; Ryder, 1991; Snyder et al., 1992; Shih et al., 2005). This led to the hypothesis of a global lunar magma ocean (LMO) as a consequence of the giant impact Moon-forming event during the first 70 to 110 Myr of solar system history (Touboul et al., 2007; Halliday, 2008; Kleine et al., 2009; Jacobson et al., 2014). As LMO crystallization progressed to ~80%, plagioclase became a liquidus phase and buoyantly floated to the top to form primordial lunar crust. Ferroan anorthosites (FANs) are proposed to be fragments of this first lunar crust. Reported FAN crystallization ages range from 4.536 ± 0.12 Ga to 4.436 ± 0.03 Ga (Alibert et al., 1994; Borg et al., 1999; Nyquist et al., 2006), consistent with an early Moon formation age. However, other FAN samples have been reported as young as 4.29 ± 0.06 Ga (62236) and 4.360 ± 0.003 Ga (60025) requiring later lunar crust formation (Borg et al., 1999, 2011). If these younger ages better define the timing of lunar crustal formation through rapid crystallization of the LMO, the Moon formation age could be as late as 150 to 200 Myr after the onset of solar system formation (OSSF, 4.569 Ga,

* Corresponding author. Tel.: +1 713 743 3399.
E-mail address: clmcleod@central.uh.edu (C.L. McLeod).

http://dx.doi.org/10.1016/j.epsl.2014.04.007
0012-821X/

Bouvier et al., 2007), compared to the currently favored time 70 to 100 Myr. Alternatively, these ages may instead provide a record of sustained crustal formation on the Moon from a number of different mechanisms.

The short-lived radioactive decay of ^{146}Sm to ^{142}Nd, with a half-life of 103 Myr (proposed recently to be revised to 68 ± 7 Myr, Kinoshita et al., 2012) can be used to evaluate lunar formation and early differentiation as fractionation of Sm/Nd in the first 300 to 500 Myr after OSSF is recorded by variations in ^{142}Nd/^{144}Nd. Previous work on lunar mare basalts show correlated ^{142}Nd/^{144}Nd–^{143}Nd/^{144}Nd variations (Nyquist et al.,, 1995; Rankenburg et al., 2006; Boyet and Carlson, 2007; Brandon et al., 2009; Gaffney and Borg, 2014). This coupled relationship has been interpreted as an isochron with an age of *ca*. 215–255 Myr (i.e. 4.355 to 4.314 Ga) after OSSF and can be explained by at least four plausible scenarios. First, the Moon formed late, close to the time of mare basalt source closure age (Borg et al., 2013). Second, Sm–Nd isotopes record late closure times of the Low-Ti, High-Ti and KREEP mantle source reservoirs via protracted differentiation following early formation of LMO cumulates (∼4.5–4.45 Ga, Nemchin et al., 2009). Third, the closure time represents a Moon-wide event that resulted in remelting of the crust coupled with resetting of Sm–Nd in the lunar mantle. Fourth, the linear relationship defined by the well-correlated ^{142}Nd–^{143}Nd systematics instead represents a mixing line with no age connotations (Münker, 2010). To further evaluate these potential scenarios and to examine how the mare basalt mantle source reservoirs are related to the timing of LMO crystallization, primordial lunar crust formation, and ultimately, the formation age of the Moon and its bulk composition, this study reports new high-precision ^{142}Nd/^{144}Nd isotope data for nine Apollo 12 samples and one Apollo 17 sample. In addition, two Apollo 15 and two Apollo 17 samples measured by Brandon et al. (2009) were re-measured here to assess data reproducibility between the two studies. Furthermore, the samples chosen for this study cover a wider petrological range exhibited by Apollo mare basalts than previous studies. This approach is necessary in order to comprehensively investigate the issues outlined above.

2. Samples

The samples studied here crystallized between 3.85 and 3.20 Ga (Nyquist et al., 1977; Rankenburg et al., 2006; Boyet and Carlson, 2007; Brandon et al., 2009; Meyer, 2009). Samples include Apollo mare basalt KREEP (Potassium, Rare Earth Element, Phosphorus-rich, 15386), Low-Ti (15555) and High-Ti (74274) compositional types. The KREEP source reservoir is inferred to represent late-stage, residual melts of LMO crystallization and is complementary to the earlier formed mafic cumulates, from which the Low-Ti and High-Ti mare basalts are derived (Snyder et al., 1997; Shearer et al., 2006). The Low-Ti mare basalts (<∼5 wt.% TiO_2, e.g. sample 15555) are thought to have been generated by partial melting of olivine and orthopyroxene cumulates (Giguere et al., 2000) although to account for observed Eu anomalies and Mg/Fe ratios, a hybrid source containing a small percentage of ilmenite has been inferred (Ryder, 1991). These cumulates are inferred to comprise at least 70% of the cumulate pile, consistent with the fact that 80% of mare basalts contain <5 wt.% TiO_2 (Giguere et al., 2000). The High-Ti reservoir is inferred to have formed from dynamic mixing of ilmenite and clinopyroxene bearing cumulates and the earlier formed Low-Ti reservoir (Hess and Parmentier, 1995; Lucey et al., 2006, e.g. sample 74275). Ilmenite saturation would not have occurred until >90% LMO solidification and is thus consistent with the relative rarity of High-Ti mare basalts (Giguere et al., 2000).

Additional samples span the mineralogic and compositional range exhibited by the Apollo 12 suite and include ilmenite basalts with moderate TiO_2 contents (2.8–5.2 wt.%) pigeonite basalts, feldspathic basalts, and olivine basalts. The olivine, feldspathic and pigeonite basalts have TiO_2 contents overlapping the Low-Ti Apollo 15 basalts (samples 12009, 12011, 12018, 12035, 12038, 12040, 12075), and likely derived from similar parental magmas, from a source consisting of 48% olivine, 22% pigeonite and 30% clinopyroxene (Papike et al., 1976; Neal et al., 1994). The ilmenite basalts are petrogenetically unrelated to the other Apollo 12 mare basalts (12005, 12022, Nyquist et al., 1979) and are inferred to have formed through variable partial melting (2–8%) of a 45.5% olivine, 42.5% pigeonite, 11.5% clinopyroxene and 0.5% plagioclase source (Neal et al., 1994). The composition of the ilmenite basalts requires subsequent crystal fractionation and accumulation.

3. Analytical techniques

Details of the Sm–Nd chemical purification techniques and analytical protocols are presented elsewhere (Debaille et al., 2007; Brandon et al., 2009). In brief, samples were processed targeting 1200–1500 ng of Nd for high-precision ^{142}Nd analyses. Powders were dissolved in HF–HNO_3 in Parr digestion vessels for 48 h at 150 °C then redissolved in HNO_3 and HCl. From these solutions, a 5 volume % aliquot was removed and spiked with a mixed ^{149}Sm–^{150}Nd spike. The samples were centrifuged and no precipitates were observed at the time of removal of these aliquots for spiking. Unspiked and spiked samples were passed through cation exchange chromatography to isolate REE's, then through a LN-spec resin to separate Sm and Nd. Solvent extraction was applied to the unspiked Nd cuts to remove ^{142}Ce which interferes on ^{142}Nd (Rehkämper et al., 1996). Cation exchange chromatography followed to remove Na introduced as $NaBrO_3$ to oxidize Ce during solvent extraction. This was followed with a second pass through an LN-spec resin to further purify the unspiked Nd cut. Yields on the unspiked Nd cuts were typically 90%. Total procedural blanks for Sm and Nd were <40 pg and <100 pg, respectively.

Spiked Nd aliquots and unspiked Sm, Nd cuts were loaded with phosphoric acid on a double Re-filament configuration, one for ionization and one for sample evaporation. Neodymium isotope analyses were carried out on a Triton Plus thermal ionization mass spectrometer (TIMS) at the University of Houston (UH). Neodymium isotopic compositions were corrected for mass fractionation using the exponential law with ^{146}Nd/^{144}Nd = 0.7219. Spiked Nd aliquots were measured on the TIMS in static mode with beam sizes on ^{143}Nd during sample runs of 0.25–0.5 V over 180–360 cycles. Spiked Sm aliquots were measured on the Nu-Plasma II ICPMS at UH using sample-standard bracketing. Repeat analysis of the Ames standard (10–35 ppb) throughout the analytical campaign yielded ^{149}Sm/^{152}Sm of 0.516863 ± 0.000054 (2σ, $n = 29$). Sm and Nd isotope dilution data are presented in Table 1.

High-precision Sm isotope analyses on unspiked aliquots were measured on the TIMS in static mode during one analytical campaign. Sample loads for Sm ranged from 100–600 ng and were 100 ng for the Ames standard. Beam sizes were 3–4 V for 360–540 cycles. The Sm isotopes were corrected for mass fractionation using the exponential law with ^{147}Sm/^{152}Sm = 0.560828 (Wasserburg et al., 1981; Brandon et al., 2009). Internal precision on ε^{149}Sm and ε^{150}Sm for samples and standards is equal to or better than ±0.08 and ±0.12, respectively (all uncertainties in this paper are $\pm 2\sigma$). The ε^{149}Sm data are reported in Table 2. All other high-precision Sm-isotope data is presented in the Supplementary Information.

High-precision Nd measurements were acquired using a 3 line multistatic routine with amplifier rotation between blocks (Caro et al., 2006). Cerium and Sm interferences on Nd were monitored with ^{140}Ce and ^{147}Sm. For samples, the ^{142}Ce interference on ^{142}Nd/^{144}Nd ranged from 0.1 ppm to 22 ppm. For standards, ^{142}Ce was consistently <0.3 ppm. High-precision Nd isotope data were collected in two analytical campaigns: April–May 2013; July–August 2013. The Ames standard was measured throughout with

Table 1
The Sm, Nd and $^{143}Nd/^{144}Nd$ values for the lunar basalts presented in this study. All data was acquired by isotope dilution on a 5% aliquot extracted after whole sample dissolution (see text). No spiked aliquots for 15555, 15386 and 70017, 74275 were analyzed by this study.

Sample	Pétrographie type	Age (Ma)	Sm (ppm)	Nd (ppm)	$^{147}Sm/^{144}Nd$	$^{143}Nd/^{144}Nd$	$\pm 2\sigma$	$\varepsilon^{143}Nd$	$\varepsilon^{143}Nd$ corr.	$\varepsilon^{143}Nd_i$
12005	*Ilmenite Basalt*	3250	2.67	7.28	0.222156	0.5135531	0.0000006	17.97	18.19	7.46
12009	*Low-Ti Olivine Basalt*	3300	3.72	10.81	0.208192	0.5130428	0.0000006	7.73	7.84	2.85
12011	*Pigeonite Basalt*	3200	4.54	13.01	0.211083	0.5130184	0.0000060	7.44	7.57	1.87
12018	*Olivine Basalt*	3300	3.32	9.64	0.208558	0.5130593	0.0000006	8.41	8.55	3.41
12022	*Ilmenite Basalt*	3270	5.07	13.31	0.230602	0.5138507	0.0000009	20.74	20.94	6.58
12035	*Olivine Basalt*	3200	4.14	11.70	0.214090	0.5132880	0.0000010	11.85	11.85	4.80
12038	*Feldspathic Basalt*	3300	5.84	18.68	0.188901	0.5123997	0.0000004	−4.65	−4.39	−1.19
12040	*Olivine Basalt*	3300	2.24	6.25	0.217283	0.5133103	0.0000009	12.28	12.62	3.78
12075	*Olivine Basalt*	3300	3.41	11.08	0.209426	0.5130343	0.0000011	8.03	8.21	2.70
70215	*High-Ti Basalt*	3720	5.46	16.08	0.246224	0.5140418	0.0000012	27.37	27.38	3.47
15555[a]	*Olivine Basalt*	3320	2.57	7.81	0.198786	0.5128394	0.0000009	3.95	4.00	3.00
15386[a]	*KREEP*	3850	31.60	112.70	0.169638	0.5118252	0.0000016	−15.84	−15.53	−2.23
74275[a]	*High-Ti Basalt*	3720	8.35	20.47	0.248158	0.5142512	0.0000014	31.49	31.51	6.71
70017[a,b]	*High-Ti Basalt*	3720	6.24	14.66	0.254915	0.5143766	0.0000009	33.85	33.87	6.05

[a] Values shown here are from Brandon et al. (2009) and are included for completeness. Measured $^{143}Nd/^{144}Nd$ values were re-normalized using a La Jolla value of 0.511847 (UH Triton) to 0.51186 (Amelin and Rotenberg, 2004). This corresponds to present-day CHUR $^{147}Sm/^{144}Nd = 0.1964$ and $^{143}Nd/^{144}Nd = 0.512637$. Reported $\varepsilon^{143}Nd$ are 10^4 parts deviation from present-day CHUR. Reported $\varepsilon^{143}Nd$ corr. values have been corrected for neutron fluence effects through the approach discussed in the text and the Supplementary Information. Reported $\varepsilon^{143}Nd_i$ ratios are calculated relative to CHUR at the time of crystallization constrained by the ages stated.

[b] Recalculated from Brandon et al. (2009).

Table 2
Summary of $\varepsilon^{149}Sm$, $^{142}Nd/^{144}Nd$ and $^{145}Nd/^{144}Nd$ isotopic data. Uncertainties stated are $\pm 2\sigma$ in the 7th decimal place. Uncorrected and neutron fluence corrected data are shown. "rpt" denotes a repeat measurement.

Sample	$\varepsilon^{149}Sm$	$^{142}Nd/^{144}Nd$	$\pm 2\sigma$ (ppm)	$\mu^{142}Nd$	$\mu^{142}Nd$ corr.	$\pm 2\sigma$ (ppm)	$\mu^{145}Nd$	$\mu^{145}Nd$ corr.	$\pm 2\sigma$ (ppm)
12005	−23.6	1.1418347	15	−2.3	9.5	1.3	−14.1	1.1	1.0
12009	−11.2	1.1418325	15	−4.2	1.4	1.3	−7.2	0.0	1.0
12011	−13.4	1.1418319	16	−4.8	2.0	1.4	−10.1	−1.5	1.1
12018	−14.5	1.1418296	15	−6.8	0.4	1.3	−13.1	−3.8	0.9
12022	−21.0	1.1418410	20	3.2	13.8	1.8	−16.0	−2.5	1.4
12022 (rpt)	–	1.1418449	27	2.5	13.1	2.7	−18.2	−4.7	2.0
12035	−21.0	1.1418338	25	−7.2	3.3	2.2	−13.8	−0.3	1.7
12038	−27.4	1.1418121	18	−22.1	−8.3	1.6	−15.2	2.5	1.1
12040	−36.1	1.1418285	23	−11.8	6.3	2.0	−23.3	−0.1	1.7
12075	−19.2	1.1418287	30	−7.6	2.0	2.6	−12.0	0.38	2.0
15555[a]	−5.7	1.1418358	30	−5.4	−2.6	2.6	−4.0	−0.6	2.0
15386[a]	−32.2	1.1418068	24	−30.9	−14.8	2.1	−18.3	0.8	1.7
70017	−1.6	1.1418571	21	17.3	18.4	1.8	−1.5	0.1	1.2
70215	−0.9	1.1418503	28	7.3	7.7	2.6	−2.6	−1.9	2.0
74275	−1.9	1.1418569	21	17.2	18.2	1.8	−2.0	−0.5	1.4

[a] Values shown here are from Brandon et al. (2009) and are included for completeness.

each dataset normalized to the average standard values for each particular campaign. For standards and samples, beam sizes were 4–6 V on ^{142}Nd for 540–1080 multistatic cycles. From campaign 1, Ames standard $^{142}Nd/^{144}Nd = 1.1418373 \pm 0.0000045$, 2σ, $n = 14$ (2SD on $\mu^{142}Nd$: ±3.9), from campaign 2, $^{142}Nd/^{144}Nd = 1.1418420 \pm 0.0000038$, 2σ, $n = 4$ (2SD on $\mu^{142}Nd$: ±3.3). High-precision Nd isotope data for samples run during this study are presented in Table 2.

4. Results

4.1. Neutron fluence corrections

Exposure of lunar samples to galactic cosmic rays promotes the production of neutrons. These neutrons are subsequently absorbed by other atoms and shift the isotopic compositions of samples (Lingenfelter et al., 1972; Nyquist et al., 1995; Boyet and Carlson, 2007; Rankenburg et al., 2006; Brandon et al., 2009). The reaction $^{149}Sm\ (n,\gamma)^{150}Sm$ is used to monitor the neutron fluence on Nd because ^{149}Sm has a large effective thermal neutron absorption cross section (Nyquist et al., 1995). The thermal neutron fluence (Ψ, in n/cm^2) a sample has received can be calculated using the measured $\varepsilon^{149}Sm$ and the σ_{eff} of ^{149}Sm:

$$\Psi = \varepsilon^{149}Sm/\left(-1^{*}\left(10^{4} \times \sigma_{eff}\right)\right)$$

The effect on Nd isotopes by epithermal neutrons (Ξ) must also be constrained. Using ^{149}Sm–^{150}Hf systematics, Sprung et al. (2013) demonstrated that each Apollo landing site has experienced a different dose of neutron fluence resulting in different Ψ/Ξ. The values of Ψ/Ξ obtained were 1.1, 0.98 and 1.5 for Apollo landing sites 12, 15 and 17, respectively (Sprung et al., 2013). These were used in the equations of Nyquist et al. (1995) and exponential law fractionation corrections to correct ^{142}Nd, ^{143}Nd, ^{144}Nd, ^{145}Nd, and ^{146}Nd. The ^{149}Sm σ_{eff} of 71,627 barns was used here and in Brandon et al. (2009) and Sprung et al. (2013), which is the most up to date value from available nuclear data (Rankenburg et al., 2006).

The $\varepsilon^{149}Sm$ of the lunar basalts studied here range from -0.9 ± 0.1 to -36.1 ± 0.1 (Table 2) and plot as a line for $^{150}Sm/^{152}Sm$ versus $^{149}Sm/^{152}Sm$ with a slope of −1.0032 (Fig. 1), confirming that the observed variation results from neutron fluence. The reported $\varepsilon^{149}Sm$ values obtained here agree with those in previous studies. For 74275, this study obtained $\varepsilon^{149}Sm = -1.9$ compared to −1.8 of Brandon et al. (2009). For 12038, this study obtained $\varepsilon^{149}Sm = -27.4$, compared to −27.0 and −27.1 of Nyquist et al. (1995) and Boyet and Carlson (2007), respectively. The smallest neutron corrections are applied to Apollo 17 samples, which have the lowest $\varepsilon^{149}Sm = -1.9$, −1.6 and −0.9 for 74275, 70017 and 70215, respectively. For Apollo 15 samples, no new high precision Sm iso-

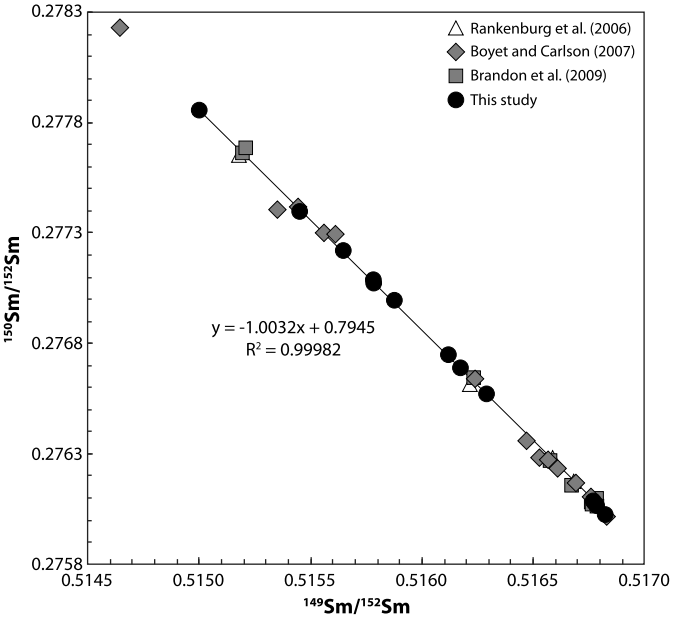

Fig. 1. Graph showing $^{150}Sm/^{152}Sm$ vs. $^{149}Sm/^{152}Sm$ for all data reported by previous high-precision Nd isotope studies and the new data acquired by this study (Table 2). New data defines a slope of −1.0032 demonstrating the effects of neutron capture on ^{149}Sm. Considering all high-precision Sm isotope data to date, a slope of −1.0054 is defined (not shown). All data normalized to $^{147}Sm/^{152}Sm = 0.560828$. Although not an issue here, it should be noted that the production of ^{152}Sm can arise from neutron capture on ^{151}Eu as reported for plagioclase rich samples (e.g. FAN 62236, Borg et al., 1999).

topic analyses were acquired. Brandon et al. (2009) obtained −5.7 for 15555, consistent with previously reported values of −6.2, −5.3 and −5.0 (Nyquist et al., 1995; Rankenburg et al., 2006; Boyet and Carlson, 2007). For KREEP sample 15386, Brandon et al. (2009) reported $\varepsilon^{149}Sm = -32.3$, consistent with values of −31.6 and −32.5 of Nyquist et al. (1995) and Rankenburg et al. (2006), respectively. For Apollo 12 samples, $\varepsilon^{149}Sm$ ranges from −11.2 to −36.1 (Table 2).

4.2. Sm–Nd

For Apollo 12 samples, measured $^{147}Sm/^{144}Nd$ ratios range from 0.1889 to 0.2306 (Table 1). For sample 12038, the measured $^{147}Sm/^{144}Nd$ of 0.1889 compares to 0.1864 obtained by Boyet and Carlson (2007). For 15555 and 15386, the measured $^{147}Sm/^{144}Nd$ ratios from Brandon et al. (2009) are used, 0.1988 and 0.1696, respectively, as both studies used fractions of the same homogenized powder of each sample. These are consistent with previously reported values of 0.2017 and 0.1988 for 15555 (Rankenburg et al., 2006; Boyet and Carlson, 2007) and 0.1681 and 0.1699 for 15386 (Carlson and Lugmair, 1979; Rankenburg et al., 2006). Sample 70215 has not been previously analyzed and has $^{147}Sm/^{144}Nd = 0.2462$. This is similar to values reported for High-Ti mare basalts ranging from 0.2470 to 0.2681 (Rankenburg et al., 2006; Boyet and Carlson, 2007; Brandon et al., 2009). From all high-precision Nd isotopic studies of Apollo samples to date, $^{147}Sm/^{144}Nd$ ratios range from 0.1688 for KREEP sample 14310 (Boyet and Carlson, 2007) to 0.2681 for High-Ti sample 70017 (Rankenburg et al., 2006).

Calculated $\varepsilon^{143}Nd_i$ values for Apollo 12 samples range from -1.2 ± 0.6 to $+7.5 \pm 0.6$ (12038 and 12005 respectively). Sample 12038 previously analyzed by Boyet and Carlson (2007) who reported $\varepsilon^{143}Nd_i = -0.4$ is similar to -1.2 ± 0.6 in this study. No comparable data are available for the remaining Apollo 12 samples of this study. For samples 15555, 15386 and 74275, previously published $\varepsilon^{143}Nd_i$ values from Brandon et al. (2009) are used in conjunction with new $\mu^{142}Nd$ data to later assess coupled $\varepsilon^{143}Nd$–$\mu^{142}Nd$ isotopic systematics. Reported values by Brandon et al. (2009) are consistent with previous and recently published data. For 15555, $\varepsilon^{143}Nd_i = +3.0 \pm 0.6$ compares well with +2.9, +2.3, and +2.3 of Rankenburg et al. (2006), Boyet and Carlson (2007), and Sprung et al. (2013), respectively. For 15386, $\varepsilon^{143}Nd_i = -2.2 \pm 1.1$ is similar to −1.2 of Rankenburg et al. (2006). For 74275, $\varepsilon^{143}Nd_i = +6.7 \pm 1.3$ is similar to +5.8 of Rankenburg et al. (2006) and +6.8 of Sprung et al. (2013), respectively. For sample 70017, previous studies report $\varepsilon^{143}Nd_i$ of +6.5, +7.1 and +6.5 (Rankenburg et al., 2006; Boyet and Carlson, 2007; Sprung et al., 2013, respectively). On further inspection of the data reported by Brandon et al. (2009), the reported value of +4.81 was found to be incorrectly calculated. Recalculation of $\varepsilon^{143}Nd_i$ gives $+6.0 \pm 1.3$, which is consistent with previously reported values. This value is used in conjunction with new $\mu^{142}Nd$ data for sample 70017 throughout this study.

The measured $^{145}Nd/^{144}Nd$ value is used as an independent monitor of applied neutron fluence corrections because ^{145}Nd has a epithermal resonance integral of 231 barns and is much larger than those for ^{142}Nd, ^{144}Nd, and ^{146}Nd (Brandon et al., 2009). If the corrections are accurate, all corrected $\mu^{145}Nd$ data will plot within the uncertainty of terrestrial standard $\mu^{145}Nd$ value, and do (Fig. S1). This also confirms the accuracy of recently reported Ψ/Ξ ratios (Sprung et al., 2013) for the three Apollo sites applied to Nd and Hf isotopes.

The neutron fluence corrected $\mu^{142}Nd$ data obtained in this study for samples 15386, 15555, 70017 and 74275 of -14.9 ± 1.7, -2.6 ± 2.0, $+18.4 \pm 1.8$ and $+18.2 \pm 1.8$ respectively compare well to -15.1 ± 1.6, -3.2 ± 6.2, $+14.4 \pm 0.9$ and $+17.1 \pm 1.8$, respectively, obtained by Brandon et al. (2009). Sample 70215 was not analyzed by previous studies and has a $\mu^{142}Nd$ of $+7.7 \pm 2.6$. For the Apollo 12 suite, the ilmenite basalts 12005 and 12022, exhibit higher $\mu^{142}Nd$ of $+9.4 \pm 1.3$ to $+13.8 \pm 1.8$, respectively, than the olivine, feldspathic, and pigeonite basalts (12009, 12011, 12018, 12035, 12038, 12040, 12075) that range from -8.3 ± 1.6 to $+6.3 \pm 2.0$). The corrected $\mu^{142}Nd$ for Apollo 12 samples here range from −8.3 to +13.8 (22.1 ppm range). The range for all samples is 38.4 ppm, with $\mu^{142}Nd$ ranging from −20.2 to +18.2 (Table 2).

Neutron fluence corrected $\mu^{142}Nd$ versus $^{147}Sm/^{144}Nd_{measured}$ define a positive correlation (Fig. 2). All data has been corrected for the effects of neutron fluence using the same model. On average, the static data of Boyet and Carlson (2007) and Rankenburg et al. (2006) are systematically displaced to higher and lower $\mu^{142}Nd$, respectively (not shown), for a given $^{147}Sm/^{144}Nd$ (Brandon et al., 2009). The multidynamic data of Boyet and Carlson (2007) are in good agreement with both the new multistatic data presented here and those from Brandon et al. (2009). This confirms the conclusion of Brandon et al. (2009) that multistatic and multidynamic analytical methods are more reproducible and likely, more accurate, than previously published static data. With the exception of sample 70215, using all other multistatic data from here, Boyet and Carlson (2007) and Brandon et al. (2009), the correlation of $\mu^{142}Nd$ vs. $^{147}Sm/^{144}Nd_{measured}$ has $R^2 = 0.94$.

5. Discussion

5.1. Coupled $\varepsilon^{143}Nd$–$\mu^{142}Nd$ isotopic systematics

The coupled ^{142}Nd–^{143}Nd isotopic system is used here to assess the timescales of early lunar differentiation. Although each previously published $\mu^{142}Nd$ dataset for Apollo mare basalts reports systematically different absolute values for a given sample, or mare basalt petrologic type, what is consistent to date is that similar slopes in $^{142}Nd/^{144}Nd$–$^{143}Nd^{144}Nd$–$^{147}Sm/^{144}Nd$ isotopic space are defined for all lunar mare basalts. This relationship can be

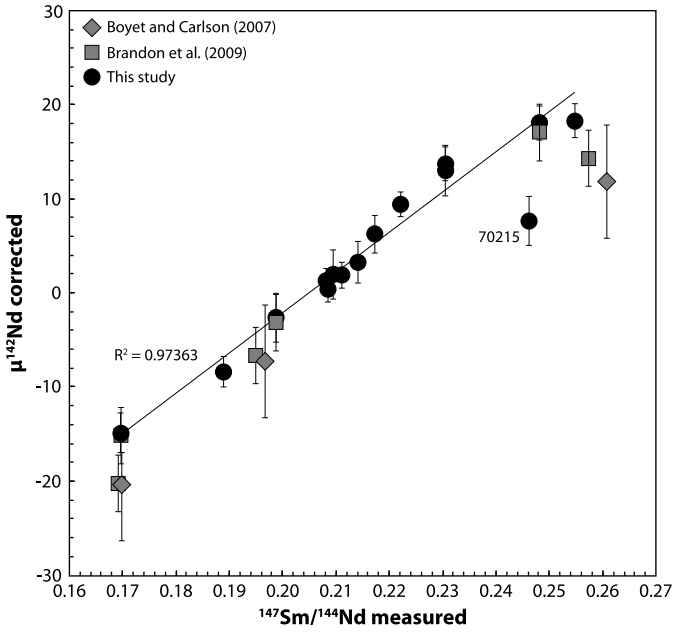

Fig. 2. Graph showing $^{147}Sm/^{144}Nd_{measured}$ vs. $\mu^{142}Nd_{corrected}$ (corrected for neutron fluence) for data of this study (solid circles) and previously reported multistatic $^{142}Nd/^{144}Nd$ datasets. Data in this study is corrected for neutron fluence effects using ^{149}Sm $\sigma_{eff} = 71{,}627$ barns and Ψ/Ξ ratios specific to each Apollo landing site (see text, Sprung et al., 2013). Considering data from this study, excluding 70215, $R^2 = 0.97$.

interpreted as a Sm–Nd source closure age or as a mixing line between end-member source components. Nyquist et al. (1995) derived a Sm–Nd lunar mantle isochron of 4.33 Ga. This is consistent with the 4.35^{+23}_{-21} Ga age obtained by Rankenburg et al. (2006), the 4.32^{+30}_{-25} Ga age obtained by Boyet and Carlson (2007) and the 4.34^{+24}_{-20} Ga age reported by Brandon et al. (2009). Most recently Gaffney and Borg (2014) reported an age of 4.36^{+31}_{-39} Ga. The age defined by the calculated lunar mantle source isochron in each case depends on how the source Sm/Nd was modeled and which source Sm/Nd ratios were used. During assessment of the Sm–Nd isotope data, a ^{146}Sm half-life of 103 Myr was used. The half-life of ^{146}Sm was recently revised to 68 Myr (Kinoshita et al., 2012). The ages presented in the models and figures that follow, were calculated using the 103 Myr half-life as recent examination of concordant isochrons in planetary bodies is most consistent with this ^{146}Sm half-life (Borg et al., 2013, 2014). Model ages calculated using the 68 Myr half-life are also listed and presented in Table 3. The reasoning behind, and justification for, the model input parameters are given in the Supplementary Information, Rankenburg et al. (2006) and in Brandon et al. (2009).

The key issue regarding the slope defined by $\mu^{142}Nd$ versus source $\varepsilon^{143}Nd$ obtained by previous studies is whether it defines an isochronous relationship, and therefore a single closure age for the mare basalts mantle source reservoirs, or instead represents a mixing line with no age implications. One reason for extending the Apollo sample selection in this study to incorporate a wider range of mare basalt petrological types was to determine whether or not a linear relationship would remain or whether greater scatter for $\mu^{142}Nd$ versus source $\varepsilon^{143}Nd$ would be revealed. If scatter, then this would demonstrate that the lunar mantle isochron ages for the Sm–Nd system obtained by previous studies were unsupported and that early differentiation of the Moon was more complex with multiple stages of Sm/Nd fractionation (e.g. Münker, 2010; Sprung et al., 2013). This is evaluated in detail here employing the new data obtained by this study.

Fig. 3 shows $\varepsilon^{143}Nd$ for the lunar mantle source reservoirs at present day plotted against $\mu^{142}Nd$ for samples of this study and Brandon et al. (2009) for 3 separate models. In Model 1, bulk Moon is considered to have average chondritic $^{147}Sm/^{144}Nd$ of 0.1964, present-day $\mu^{142}Nd = -20$ (Boyet and Carlson, 2005) and $^{146}Sm/^{144}Sm$ of 0.008 at 4.569 Ga (Brandon et al., 2009). In Model 2, bulk Moon has the same average chondritic $^{147}Sm/^{144}Nd$ but with $\mu^{142}Nd = -7.3$ (Sprung et al., 2013) which is similar to some enstatite chrondrites (Gannoun et al., 2011). In Model 3 fractionation of Sm/Nd from average chondritic to superchondritic occurs at 4.538 Ga, (or 31 Myr after OSSF at 4.569 Ga) such that the bulk Moon has an initial non-chrondritic Sm/Nd composition (Brandon et al., 2009).

Present-day source $\varepsilon^{143}Nd$ for each sample is calculated using the $^{143}Nd_i$ value (i.e. at the time of crystallization) and the calculated source $^{147}Sm/^{144}Nd$ in order to directly compare the mare basalt mantle source reservoirs. Isochrons at 100 Myr intervals and constant source $^{147}Sm/^{144}Nd$ in intervals of 0.025 are shown. At the time of oldest mare basalt crystallization at 3.85 Ga (Table 1), >99.9% of ^{146}Sm had decayed away. No additional detectable changes occur in the present-day $\mu^{142}Nd$, such that the measured $\mu^{142}Nd$ data corrected for neutron fluence directly reflects that of the mare basalt source reservoir. The mantle sources for the Apollo mare basalts are defined by their $\mu^{142}Nd$ compositions with the KREEP reservoir from −15.1 to −20.2, the Low-Ti reservoir, including Apollo 12 olivine, plagioclase, and pigeonite basalts, from −8.5 to +9.4, and the High-Ti reservoir, including Apollo 12 ilmenite basalts, from +13.7 to +18.3. Importantly, in all three models, the linear relationship between measured $\mu^{142}Nd$ and source $\varepsilon^{143}Nd$, when including the new Apollo 12 mare basalt data is confirmed (Fig. 3). Each model is evaluated in the following paragraphs.

In Model 1, the bulk Moon formed with average chondritic values ($^{147}Sm/^{144}Nd$ of 0.1964 and a present day $\mu^{142}Nd = -20$, Fig. 3A). In this model, the mare basalt source reservoirs formed at different times. The High-Ti source formed at ~4.44 Ga and the KREEP source at 4.00 Ga assuming a KREEP source $^{147}Sm/^{144}Nd$ of ~0.173. This scenario, is consistent with an early-formed Moon and consequent LMO cumulate crystallization, where small amounts of late stage residual melt (KREEP) persist in the upper lunar mantle (Nemchin et al., 2009). This scenario is broadly inconsistent with independently-derived KREEP source ages constrained by ^{87}Rb–^{87}Sr, $^{238,235}U$–$^{206,207}Pb$, and ^{147}Sm–^{143}Nd of 4.3 to 4.4 Ga (Tera and Wasserburg, 1974; Carlson and Lugmair, 1979; Nyquist and Shih, 1992; Boyet and Carlson, 2007). In this chondritic model, because the High-Ti and KREEP sources formed at different times, the linear relationship would reflect reservoir mixing, not a closure age for the Sm–Nd isotopic system.

In Model 2, the bulk Moon formed with average chondritic values for $^{147}Sm/^{144}Nd$ of 0.1964 but a present day $\mu^{142}Nd = -7.3$ (Fig. 3B). This follows the suggestion by Sprung et al. (2013) that the bulk Moon, and possibly, Earth, may have $\mu^{142}Nd_i$ that are distinct from average chondrites. This potentially reflects a nucleosynthetic anomaly in precursor materials relative to average chondrites (possibly similar to some enstatite chondrites). Using these values to model source $\varepsilon^{143}Nd$–$\mu^{142}Nd$ systematics of lunar

Table 3
Summary of ages defined by the coupled $\mu^{142}Nd$–$\varepsilon^{143}Nd$ source models presented in Fig. 3.

	Model 1	Model 2	Model 3
$t_{1/2}$ $^{146}Sm = 68$ Myr	High Ti source: 4.50 Ga KREEP source: 4.10 Ga	4.45 Ga	4.41 Ga
$t_{1/2}$ $^{146}Sm = 103$ Myr	High Ti source: 4.44 Ga KREEP source: 4.00 Ga	4.39 Ga	4.34 Ga

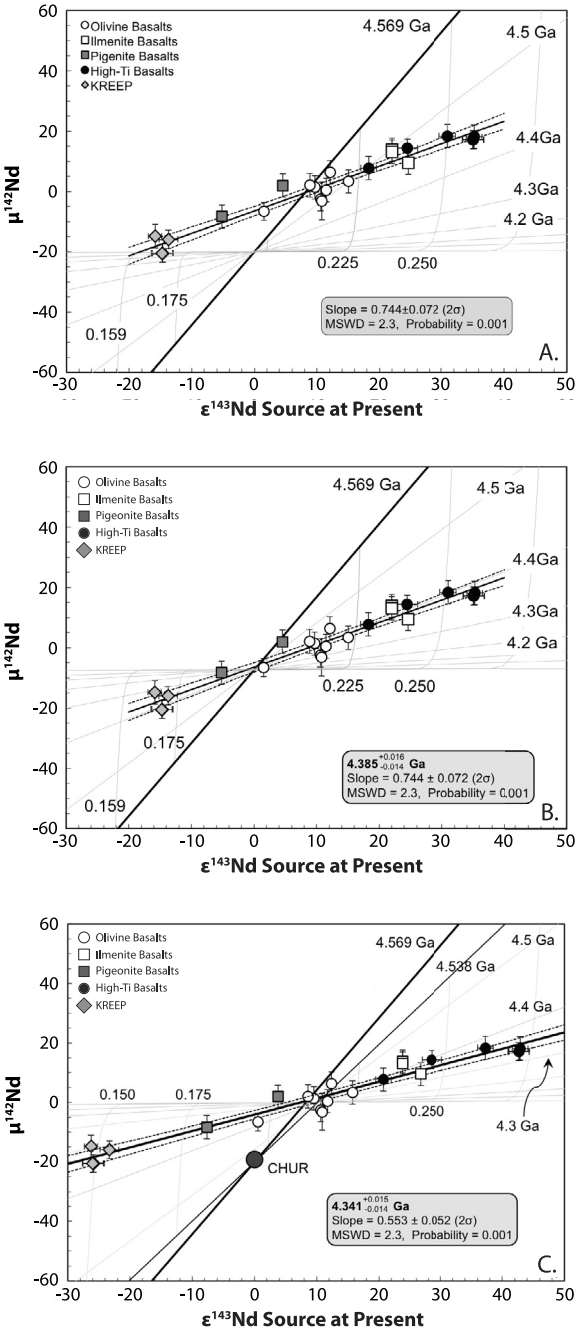

Fig. 3. Coupled ε^{143}Nd–μ^{142}Nd source models showing calculated source compositions for the multistatic data of this study and Brandon et al. (2009). The error bars for present-day ε^{143}Nd accounts for a 0.2% uncertainty on the mixed Sm–Nd spike values and the isotope dilution measurements. All sources are evolved to the present-day. All μ^{142}Nd data are presented with their $\pm 2\sigma$ error bars. For the three source models presented in this study, the initial bulk solar system ^{146}Sm/^{144}Sm = 0.008 at 4.569 Ga after Bouvier et al. (2007) is used. CHUR: Chondritic Uniform Reservoir. Constant source ^{147}Sm/^{144}Nd ratios at 0.025 intervals are shown alongside isochrons at 100 Ma intervals. The solid black line defines a regression line through the calculated source reservoirs with a $\pm 2\sigma$ error envelope (dashed lines). The equations used to produce the models presented here are discussed in Rankenburg et al. (2006), Bennett et al. (2007) and Debaille et al. (2007). A: Model 1 – Chondritic model for a bulk Moon, ^{147}Sm/^{144}Nd = 0.1964, μ^{142}Nd = −20 (present-day). B: Model 2 – Chondritic model for a bulk Moon, ^{147}Sm/^{144}Nd = 0.1964, μ^{142}Nd = −7.3 (present-day, after Sprung et al., 2013). In this scenario, lunar μ^{142}Nd$_i$ is distinct from average chondrites. C: Model 3 – Two-stage differentiation history for the Moon (after Brandon et al., 2009) in which Sm and Nd are fractionated at 4.538 Ga (31 Ma OSSF). The Moon subsequently forms from a superchondritic reservoir (^{147}Sm/^{144}Nd = 0.2136, ^{146}Sm/^{144}Sm = 0.00649). Differentiation at 4.34^{+15}_{-14} Ga generates the Low-Ti, High-Ti and KREEP source reservoirs.

mare basalts results in single closure time for the lunar mantle (Fig. 3B). This is because the linear array defined by the data intersects the Solar System isochron at μ^{142}Nd = −7.3 (Sprung et al., 2013). The Sm–Nd closure age for this lunar isochron is 4.39^{+16}_{-14} Ga (180 Myr after OSSF). Using the 68 Myr half-life for ^{146}Sm gives an age of 4.45^{+10}_{-09} (120 Myr after OSSF).

In Model 3 the data are evaluated using the two-stage model of Brandon et al. (2009). In this scenario, fractionation of Sm from Nd occurs at 4.538 Ga to produce a superchondritic reservoir with ^{147}Sm/^{144}Nd = 0.2136 and ^{146}Sm/^{144}Sm = 0.00649. This produces a present-day ε^{143}Nd of +10.2 and μ^{142}Nd of 0. This model is based on the hypothesis that collisional erosion could preferentially remove crust and thus fractionate the bulk Sm/Nd on precursor differentiated bodies that later accrete to form the Earth and the giant impactor from which the Moon formed (O'Neill and Palme, 2008). As in Model 2, using these values to model source ε^{143}Nd–μ^{142}Nd systematics of lunar mare basalts results in a single closure time for the lunar mantle (Fig. 3C). This is because the linear array intersects the 4.538 Ga isochron at μ^{142}Nd = 0, identical to the Earth's convecting mantle (Murphy et al., 2010). The closure age for this lunar isochron is 4.34^{+15}_{-14} Ga (230 Myr after OSSF). Using the 68 Myr half-life for ^{146}Sm gives an age of 4.41^{+10}_{-08} (160 Myr after OSSF). The isochron age of 4.34^{+15}_{-14} Ga is indistinguishable from the age of 4.34^{+24}_{-20} Ga obtained by Brandon et al. (2009) using the 103 Myr half-life for ^{146}Sm.

The issue of whether a chondritic model (Fig. 3A) necessitates mixing between end-member sources with different closure ages, or whether the Model 2 and 3 isochrons (Fig. 3B, C) could be explained by source mixing, requires evaluation. A multi-component mare basalt-mixing model was recently proposed by Münker (2010) as an explanation for the observed decoupling between ^{142}Nd/^{144}Nd–Sm/Nd and between ^{182}W/^{183}W–Hf/W. If correct, then the linear array defined by source ε^{143}Nd–μ^{142}Nd (Fig. 3) would be a mixing line and not an isochron. The model of Munker (2010) requires assimilation of ilmenite–clinopyroxene cumulates and a KREEP component by trace-element poor melts derived from the Low-Ti source mantle to reconcile ^{142}Nd and ^{182}W signatures with LMO crystallization at *ca.* 50 Myr after solar system formation. In Fig. 4, the end-member components for this model are plotted for measured ^{147}Sm/^{144}Nd versus μ^{142}Nd. Münker (2010) used all available μ^{142}Nd data to date to propose mixing between primitive Low-Ti melts, an ilmenite-rich reservoir and a KREEP reservoir to account for a linear array defined by ^{147}Sm/^{144}Nd versus μ^{142}Nd (Nyquist et al., 1995; Rankenburg et al., 2006; Boyet and Carlson, 2007; Brandon et al., 2009, Fig. 4A). Considering only the multistatic data from this study and Brandon et al. (2009) for reasons stated earlier, the three component mixing relationship required by the Münker (2010) model breaks down (Fig. 4A). In order to reproduce the linear relationship through multi-component mixing, the Primitive Low-Ti melt and Ilmenite-rich reservoirs require their μ^{142}Nd values to be adjusted from +20 to −10 and from +70 to +30, respectively. These −30 to −40 ppm changes in μ^{142}Nd values are inconsistent with their calculated source Sm/Nd ratios that necessitated the end-member component values proposed in Münker (2010). Source reservoir mixing is also inconsistent with the scatter defined by 1/Nd vs. μ^{142}Nd (Fig. 4B).

The mixing model of Münker (2010) is also inconsistent with models that examine mare basalt petrogenesis through mixing between the Low-Ti, High-Ti and KREEP source reservoirs as follows. First, the distinct ε^{143}Nd$_i$ and εHf$_i$ systematics of the Low-Ti and High-Ti basalts imply separate, genetically unrelated source reservoirs (Beard et al., 1998; Gaffney and Borg, 2014). Second, coupled ε^{143}Nd–ε^{176}Hf source models fail to reproduce the high Nd/Hf$_{measured}$ of the Low-Ti basalts from interaction between

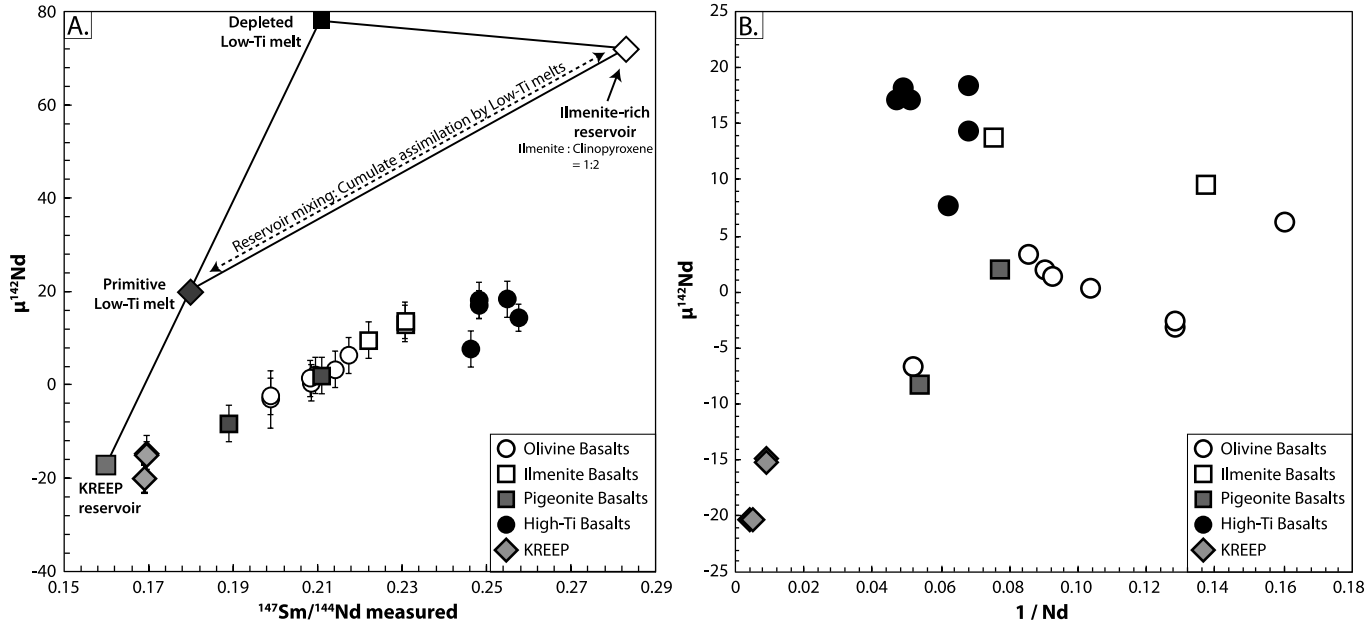

Fig. 4. A. End-member components from the mixing model of Münker (2010) plotted alongside multistatic data of this study and data from Brandon et al. (2009). As shown, the linear array defined by μ^{142}Nd vs. ^{147}Sm/^{144}Nd$_{measured}$ cannot be reconciled through multi-component mixing. For discussion see text. B. Plot of 1/Nd vs. μ^{142}Nd shows clear scatter ruling out mantle source reservoir mixing as a plausible explanation for the well-correlated trend defined by ε^{143}Nd–μ^{142}Nd signatures in the Apollo mare basalts.

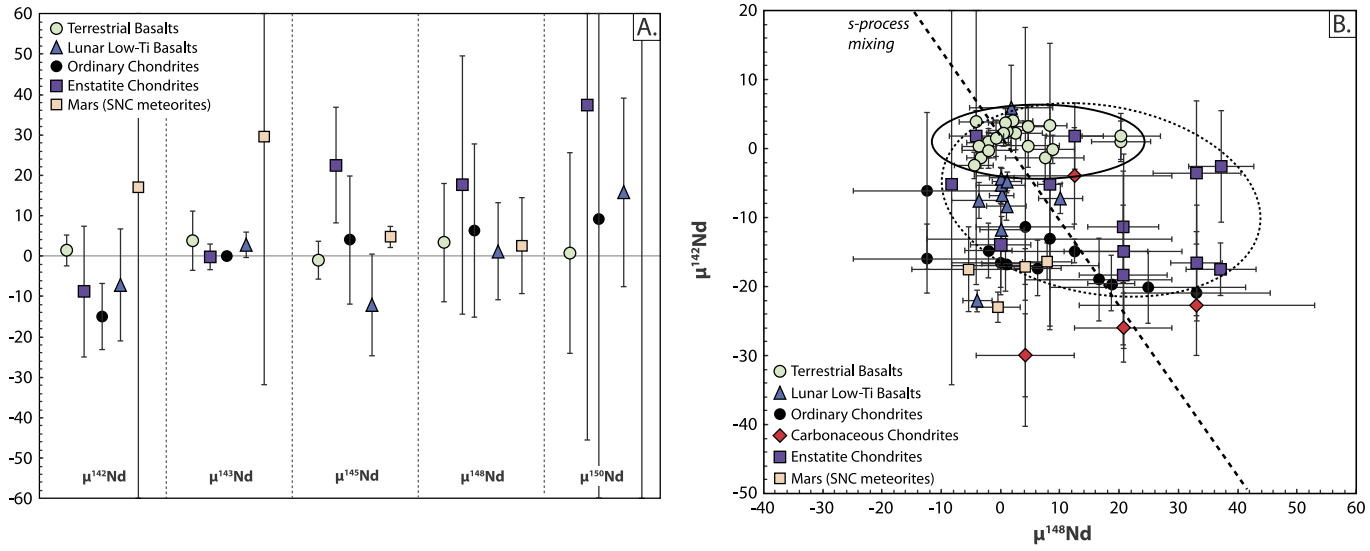

Fig. 5. A: Summary of available Nd isotope data for Terrestrial Basalts (Murphy et al., 2010); Enstatite Chondrites (Gannoun et al., 2011); Ordinary Chondrites (Boyet and Carlson, 2005; Carlson et al., 2007); SNC Meteorites (Debaille et al., 2007) and Lunar Basalts (this study, Brandon et al., 2009). For lunar samples, only Low-Ti Basalts are plotted. This suite of samples have been proposed to best represent the bulk Moon (Kleine et al., 2005; Rankenburg et al., 2006). B: μ^{142}Nd vs. μ^{148}Nd for Terrestrial Basalts, Enstatite Basalts, Carbonaceous Chondrites, Ordinary Chondrites, SNC Meteorites (not all samples plot within the compositional parameters shown) and Lunar Basalts (Low-Ti only, see text). References as in A. Carbonaceous Chondrite data from Andreasen and Sharma (2006). The dashed black line defines s-process mixing processes (Kleine et al., 2013). The terrestrial basalt (solid line) and enstatite chondrite (dashed line) data are circled in order to highlight that, to date, there is a lack of evidence in support of a nucleosynthetic origin for variations in Nd isotope signatures.

KREEP and High-Ti reservoirs or their melts (Brandon et al., 2009). Third, REE concentrations and Sr–Nd isotopic systematics demonstrate that Low-Ti and High-Ti samples within the Apollo 12 basalt suite originated from distinct source reservoirs (Nyquist et al., 1979). A mixing relationship involving the Low-Ti and KREEP reservoirs was also recently dismissed (Sprung et al., 2013). For a superchondritic Moon, and in order for the correlation in ^{147}Sm/^{144}Nd vs. ^{176}Lu/^{177}Hf source characteristics to be the result of mixing, a range of different LMO cumulates would have to mix with the KREEP reservoir in very specific proportions. For a chondritic Moon, a complex mixing model between olivine–orthopyroxene cumulates, clinopyroxene cumulates and various interstitial cumulate liquids could account for Lu/Hf, and Sm/Nd signatures of the Low-Ti mare basalts (Sprung et al., 2013).

One caveat to the interpretation of the data presented above is that the variations observed in Nd isotopes may not purely be the result of radioactive decay. Instead, observed differences are (in part) potentially nucleosynthetic in origin as a result of isotopic heterogeneity in the protoplanetary disk, as has been suggested by coupled Ti–Cr signatures (Trinquier et al., 2009). More recently, Kleine et al. (2013) proposed that differences in the Nd isotopic compositions between the Earth–Moon–Mars system and chondrites was a result of heterogeneous distribution of s- and p-process materials. Such a scenario, manifested as Model 2 above,

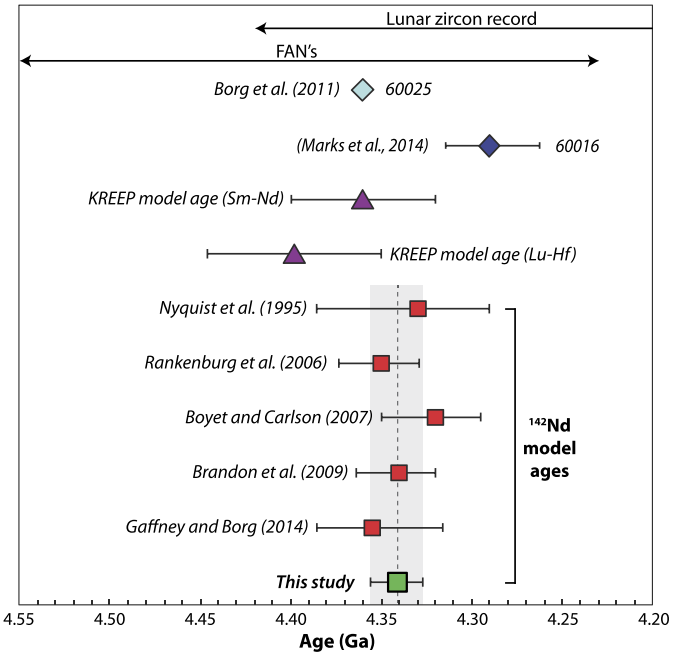

Fig. 6. A compilation of ^{142}Nd model ages for lunar basalts, including the 4.34 Ga $+15/-14$ model age from this study. KREEP source model ages are shown for comparison (Gaffney and Borg, 2013). The young ages for FAN 60025, 4.360 ± 0.003 Ga (Borg et al., 2011) and FAN 60016, $4.299 + 24$, -28 Ga (Marks et al., 2014) are also shown. Based on data available to date, the lunar zircon record and the FAN record suggest the Moon formed early during Solar System evolution. The ^{142}Nd model ages are recording the closure of the Sm–Nd isotopic system in the mare basalt mantle source reservoirs and are interpreted as recording a later event at *ca.* 4.34 Ga. The gray shaded field defines the error associated with the ^{142}Nd model age of this study. All previous studies are within error of this value. These ^{142}Nd model ages were calculated using the preferred 103 Myr half-life for ^{146}Sm following the arguments of Borg et al. (2014).

cannot be completely ruled out or advocated for Nd isotopes. Fig. 5 illustrates that at the resolution currently available, no resolvable nucleosynthetic distinctions in Nd isotopes are observed between the different inner solar system bodies.

In summary, despite the greater petrologic diversity exhibited by the Apollo 12 samples, and the distinct evolutionary history of the Low-Ti, High-Ti reservoirs and KREEP mantle source reservoirs, the high-precision, multistatic μ^{142}Nd data for lunar mare basalts define a well-correlated ε^{143}Nd–μ^{142}Nd relationship. This is best explained as an isochron and is interpreted as recording a lunar mantle closure age for the Sm–Nd system at *ca.* 4.45 to 4.34 Ga, the absolute value of which depends on the μ^{142}Nd of the bulk Moon and which of the half-lives for ^{146}Sm is used (68 or 103 Myr). As discussed, this relationship does not reflect multi-component mixing. This conclusion is consistent with, and reaffirms the interpretations reported by previous Sm–Nd isotope studies of mare basalts, despite the different evolution models that each study proposed (Fig. 6; Nyquist et al., 1995; Rankenburg et al., 2006; Boyet and Carlson, 2007; Brandon et al., 2009; Gaffney and Borg, 2014).

5.2. Potential origins of the mare basalt ^{142}Nd–^{143}Nd source closure age

In the previous section, the possibility that the linearity between source ^{142}Nd–^{143}Nd for the mare basalts resulted from mixing was eliminated. The alternative interpretation is that it represents a Sm–Nd mantle closure age as early as 4.45 to as late as 4.34 Ga (Fig. 6), depending on the μ^{142}Nd of the bulk Moon and which ^{146}Sm half-life is used. Model ages using I–Xe, Hf–W and U–Pb isotope systems and recent *N*-body simulations constrain the Moon-forming giant impact to 70–110 Myr after solar system formation (Ozima and Podosek, 1999; Touboul et al., 2007; Halliday, 2008; Jacobson et al., 2014). If the ^{146}Sm half-life of 68 Myr is correct and the Moon has a bulk μ^{142}Nd today of -7.3 (Model 2 above), then the mare basalt mantle source closure time of 4.45^{+10}_{-9} Ga appears to be consistent with the presently accepted age of the Moon. In all other scenarios where the ^{146}Sm half-life of 103 Myr is used, or the Moon has a bulk μ^{142}Nd of 0 (Model 3 above), then the mare basalt mantle source closure time ranges from 4.41^{+10}_{-08} to 4.34^{+15}_{-14}, and 50 to 160 Myr later than the presently accepted formation time of the Moon. From these constraints, the later closure time for the mare basalt sources could result from protracted differentiation of the LMO, remelting of the crust and resetting of the mare basalt mantle sources via a Moon-wide event, or instead indicates that the Moon formed later than presently believed. These scenarios are evaluated below.

First, a late formation age for the Moon at 4.41 to 4.34 Ga is consistent with recent ages determined for FAN's of 4.36 ± 0.003 Ga for 60025 and 4.29^{+24}_{-28} Ga for 60016, if these FAN's represent primordial lunar crust (Fig. 6; Borg et al., 2011; Marks et al., 2014). This scenario also depends on whether the FAN ages $>$4.4 Ga, and the lunar zircon record, which currently extends back to *ca.* 4.42 Ga, are accurate or not (Fig. 6; Norman et al., 2003; Nemchin et al., 2009; Nyquist et al., 2006). However, the U–Pb ages of up to 4.4 Ga and the Hf isotopic compositions in Jack Hills zircons from Australia, have been argued as evidence in support of an early-formed Moon with mixing in the silicate Earth constrained to $\geqslant$4.4 Ga as a consequence of a Moon-forming giant impact event (Harrison et al., 2008; Valley et al., 2014).

Second, the formation of a plagioclase flotation crust has the potential to act as an insulator and significantly prolong LMO crystallization (Solomon and Longhi, 1977). In this scenario small volume melts are present within the lunar interior for hundreds of millions of years after the giant impact event. Recently, Elkins-Tanton et al. (2011) modeled 80% LMO solidification after only 1000 yrs in a scenario where a plagioclase flotation crust acted as a conductive lid. Rapid LMO crystallization is potentially supported by Lu–Hf isotopic systematics in Apollo 14 zircons, which constrain closure time of the KREEP source reservoir, and by inference, LMO crystallization to no later than 4.38 Ga (Taylor et al., 2009). In the absence of tidal heating, the remaining 20% would have crystallized within the following 10 Myr. This time of LMO solidification would not be consistent with an early-formed Moon and a late mare basalt source closure time. In a scenario where tidal heating from Earth occurs, significantly longer LMO crystallization timescales are possible (e.g. Garrick-Bethell et al., 2010; Meyer et al., 2010). For example for a time of 4.51 Ga where the LMO had solidified to a point that an anorthitic lid had formed, melt can remain extent for another 220 Myr (Meyer et al., 2010; Elkins-Tanton et al., 2011). Alternatively, melts may have been sustained within the lunar interior where lunar crustal growth was asymmetrical with circulation within the LMO preferentially oriented to the farside of the Moon due to radiative shielding caused by Earth's proximity (Loper and Werner, 2002; Garrick-Bethell et al., 2010). Either of these mechanisms to sustain melts in the lunar mantle would be consistent with the ^{143}Nd–^{142}Nd source closure age of *ca.* 230 Myr and would, in part, explain the *ca.* 500 Myr age range observed in the lunar zircon record (Fig. 6; 4.4–3.9 Ga, Nemchin et al., 2008, 2009; Taylor et al., 2009).

Third, the ^{143}Nd–^{142}Nd mantle closure age may instead represent a post LMO solidification, late-stage magmatic event during which consequent isotope requilibration of the mantle source reservoirs at *ca.* 4.34 Ga (Fig. 6; $t_{1/2}$ ^{146}Sm $=$ 103 Myr). This scenario is supported by the oldest Mg-suite norite 77215 of 4.33 Ga, the KREEP ^{147}Sm–^{143}Nd model age of 4.36 Ga, and the Apollo 17 zircons of 4.35–4.20 Ga (Fig. 6; Lugmair and Carlson, 1978; Carlson and Lugmair, 1979; Gaffney and Borg, 2013). In this

scenario, the LMO crystallized rapidly in an early forming Moon. Resetting of isotope signatures may have occurred during serial magmatism (Borg et al., 2011), during whole-scale lunar mantle overturn driven by gravitationally unstable cumulates (Hess and Parmentier, 1995; Elkins-Tanton et al., 2002), or potentially during one (or more) impacts. The effects from giant impacts may have been significant enough to disturb isotopic systematics such as that which formed the South Pole Aitken (SPA) basin which is thought to have formed from a large impact at 4.4 to 4.3 Ga (Morbidelli et al., 2012; Fernandes et al., 2013; Bottke et al., 2014). This scenario is consistent with recent models which indicate that the Moon could have melted to a depth of *ca.* 250 km during the impact which formed the SPA basin during which all of the lunar crust and a portion of the upper lunar mantle could have been removed (50% melting to 390 km, Hurwitz and Kring, 2013). The peak in the lunar zircon record at *ca.* 4.32 Ga (Grange et al., 2013) could record this remelting of the lunar interior. What remains to be tested is if this is (1) a dynamically plausible scenario and (2) whether this resulted in local, regional or global re-melting of the lunar interior.

6. Conclusions

Mare basalts from the Apollo 12, 15 and 17 collections were analyzed for their Sm–Nd isotopic systematics. Apollo 12 samples include ilmenite, pigeonite, and olivine mare basalt petrological types that have not been analyzed for high-precision $^{142}Nd/^{144}Nd$ previously. Combined with previous samples, new results allow for an assessment of the Low-Ti, High-Ti and KREEP mantle source reservoirs in the context of a single closure age for all versus a multi-stage history. The new data display a linear correlation between calculated source $\varepsilon^{143}Nd$–$\mu^{142}Nd$, demonstrating that adding a wider array of basalt compositions does not change the correlated systematics previously obtained (Nyquist et al., 1995; Rankenburg et al., 2006; Boyet and Carlson, 2007; Brandon et al., 2009). Models with three different bulk starting compositions spanning the range of potential Sm–Nd isotope systematics were used to evaluate possible Moon formation and evolution models in the context of the new $\varepsilon^{143}Nd$–$\mu^{142}Nd$ data.

A model with an average chondritic Sm/Nd leading to a present-day $\mu^{142}Nd$ of −20 gives different model ages for the KREEP and High-Ti sources and requires that the linear relationship for $\varepsilon^{143}Nd$–$\mu^{142}Nd$ is a mixing line between these two end member components. This model was eliminated because additional evaluation of compositional data for mare basalts indicates that the coupled relationship between $\varepsilon^{143}Nd$–$\mu^{142}Nd$ cannot be a mixing line. A second model with an average chondritic Sm/Nd and a present-day $\mu^{142}Nd$ of −7.3 results in an isochronous relationship and a mare basalt mantle source closure age of 4.45^{+10}_{-09} Ga using the 68 Myr half-life for ^{146}Sm and 4.39^{+16}_{-14} Ga using the 103 Myr half-life. If the 68 Myr half-life for ^{146}Sm is correct, the 4.45 Ga mare basalt source closure age is close to the estimated time of the Moon-forming giant impact. A third model that uses a superchondritic Sm/Nd present-day $\mu^{142}Nd$ of 0, similar to the Earth's present-day convecting mantle, also produces an isochronous relationship and gives source closure ages of 4.41^{+10}_{-08} Ga (using the 68 Myr ^{146}Sm half-life) and 4.34^{+15}_{-14} Ga (using the 103 Myr ^{146}Sm half-life). The second model using the longer ^{146}Sm half-life and the third model (both half lives) all result in mantle source closure ages that are much later than the presently accepted age of the Moon.

There are three possible explanations for the mare basalt mantle sources having a 4.4 Ga or later closure age. First, the crustal ages that support an early-formed Moon are inaccurate and the Moon actually formed late *ca.* 4.35 Ga. Second, the Moon formed early and residual melt in the LMO was sustained for up to 200 Myr as a result of tidal heating or asymmetric/two-stage LMO evolution. Third, the Moon formed early and the LMO crystallized rapidly. The mantle source closure age then represents remelting or resetting of the mantle Sm–Nd isotope systematics via mantle overturn or by a significant impact on the Moon for example that which formed the SPA basin. Each of these possible outcomes are supported by various observations and lunar data. Each have caveats and therefore cannot be refuted or favored at present. However, if an early formed Moon of $\geqslant$4.4 Ga is correct, consistent with zircon studies from Earth samples (Harrison et al., 2008; Valley et al., 2014), the lunar FAN and zircon record, *N*-body simulations (Jacobson et al., 2014), and if magma oceans crystallize in a few million years (Elkins-Tanton et al., 2011), then the scenario for a melting event during which the Sm–Nd isotopic systematics in the mare basalt mantle sources were reset is favored. What is clear is that the lunar mantle closed with respect to Sm–Nd isotopes at *ca.* 4.34 Ga and any lunar formation or evolution model must be able to reconcile this aspect of the lunar record.

Acknowledgements

Financial support was provided by NASA Cosmochemistry grant NNX12AD06G awarded to ADB. Rasmus Andreasen and Tom Lapen are thanked for their assistance during analysis of Sm-spiked samples on the Nu-Plasma II at UH. Comments from two anonymous reviewers helped improve the clarity and structure of this manuscript.

Appendix A. Supplementary material

Supplementary material related to this article can be found online at http://dx.doi.org/10.1016/j.epsl.2014.04.007.

References

Alibert, C., Norman, M.D., McCulloch, M.T., 1994. An ancient age for a ferroan anorthosite clast from lunar breccia 67016. Geochim. Cosmochim. Acta 58, 2921–2926.

Andreasen, Sharma, 2006. Solar nebula heterogeneity in p-process Samarium and Neodymium isotopes. Science 314, 806–809.

Beard, B.L., Taylor, L.A., Scherer, E.E., Johnson, C.M., Snyder, G.A., 1998. The source region and melting mineralogy of high-titanium and low-titanium lunar basalts deduced from Lu–Hf isotope data. Geochim. Cosmochim. Acta 62, 525–544.

Bennett, et al., 2007. Coupled ^{142}Nd–^{143}Nd isotopic evidence for Hadean mantle dynamics. Science 318, 1907–1910.

Borg, L., Norman, M., Nyquist, L., Bogard, D., Snyder, G., Taylor, L., Lindstrom, M., 1999. Isotopic studies of ferroan anorthosite 62236: a young lunar crustal rock from a light rare-earth-element-depleted source. Geochim. Cosmochim. Acta 63, 2679–2691.

Borg, L., Connelly, J., Boyet, M., Carlson, R.W., 2011. Chronological evidence that the Moon is either young or did not have a global magma ocean. Nature 477, 70–73.

Borg, L., Connelly, J., Cassata, W., Gaffney, A., Carlson, R., Papanatassiou, D., Wasserburg, J., Ramon, E., Lindval, R., Bizarro, M., 2013. Evidence for widespread magmatic activity at 4.36 Ga in the Lunar Highlands from young ages determined on Troctolite 76535. In: 44th Lunar and Planetary Science Conference #1563.

Borg, L., Brennecka, G., Marks, N., Symes, S., 2014. Neodymium isotopic evolution of the solar system inferred from isochron studies of planetary materials. In: 45th Lunar and Planetary Science Conference #1037.

Bottke, W.F., Vokrouhlicky, D., Marchi, S., Swindle, T., Scott, E.R.D., Weirich, J.R., 2014. The evolution of giant impact ejecta and the age of the Moon. In: Lunar and Planetary Science Conference #1611.

Bouvier, A., Blichert-Toft, J., Moynier, F., Vervoort, J.D., Albare`de, F., 2007. Pb–Pb dating constraints on the accretion and cooling history of chondrites. Geochim. Cosmochim. Acta 71, 1583–1604.

Boyet, Carlson, 2005. ^{142}Nd evidence for early (>4.53 Ga) global differentiation of silicate Earth. Science 309, 576–581.

Boyet, M., Carlson, R.W., 2007. A highly depleted moon or a non-magma ocean origin for the lunar crust? Earth Planet. Sci. Lett. 262, 505–516.

Brandon, A.D., Lapen, t.J., Debaille, V., Beard, B.L., Rankenburg, K., Neal, C., 2009. Re-evaluating $^{142}Nd/^{144}Nd$ in lunar mare basalts with the implications for the early evolution and bulk Sm/Nd of the Moon. Geochim. Cosmochim. Acta 73, 6421–6445.

Carlson, R.W., Lugmair, G.W., 1979. Sm–Nd constraints on early differentiation and the evolution of KREEP. Earth Planet. Sci. Lett. 45, 123–132.

Carlson, R.W., Lugmair, G.W., 1981. Sm–Nd age of lherzolite 67667: implications for the processes involved in lunar crustal formation. Earth Planet. Sci. Lett. 56, 1–8.

Carlson, et al., 2007. Chondrite Barium, Neodymium, Samarium isotopic heterogeneity and Early Earth differentiation. Science 316, 1175–1178.

Caro, G., Bourdon, B., Birck, J.-L., Moorbath, S., 2006. High-precision $^{142}Nd/^{143}Nd$ measurements in terrestrial rocks: constraints on the early differentiation of the Earth's mantle. Geochim. Cosmochim. Acta 70, 164–191.

Debaille, V., Brandon, A.D., Yin, Q.Z., Jacobsen, B., 2007. Coupled ^{142}Nd–^{143}Nd evidence for a protracted magma ocean in Mars. Nature 450, 525–528.

Elkins-Tanton, L.T., Van Orman, J.A., Hager, B.H., Grove, T.L., 2002. Re-examination of the lunar magma ocean cumulate overturn hypothesis: melting or mixing is required. Earth Planet. Sci. Lett. 196, 239–249.

Elkins-Tanton, L.T., Burgess, S., Yin, Q.-Z., 2011. The lunar magma ocean: reconciling the solidification process with lunar petrology and geochronology. Earth Planet. Sci. Lett. 304, 326–336.

Fernandes, V.A., Fritz, J., Weiss, B.P., Garrick-Bethell, I., Shuster, D.L., 2013. The bombardment history of the Moon as recorded by ^{40}Ar–^{39}Ar chronology. Meteorit. Planet. Sci. 48 (2), 241–269.

Gaffney, A.M., Borg, L.E., 2013. A young age for KREEP formation determined from Lu–Hf isotope systematics of KREEP basalts and Mg-suite samples. In: 44th Lunar Planetary Science Conference #1714.

Gaffney, A.M., Borg, L.E., 2014. Evidence for magma ocean solidification at 4.36 Ga from ^{142}Nd–^{143}Nd variation in mare basalts. In: 45th Lunar Planetary Science Conference #1449.

Gannoun, A., Boyet, M., Rizo, H., Goresy, A.E., 2011. ^{146}Sm–^{142}Nd systematics measured in Enstatite chondrites reveals a heterogeneous distribution of ^{142}Nd in the solar nebula. Proc. Natl. Acad. Sci. 108, 7693–7697.

Garrick-Bethell, I., Nimmo, F., Wieczorek, M.A., 2010. Structure and formation of the lunar farside Highlands. Science 330, 949–951.

Giguere, T.A., Taylor, G.J., Hawke, B.R., Lucey, P.G., 2000. The titanium contents of lunar mare basalts. Meteorit. Planet. Sci. 35, 193–200.

Grange, M.L., Nemchin, A.A., Pidgeon, R.T., Merle, R.E., 2013. What lunar zircon ages tell? In: 44th Lunar Planetary Science Conference #1884.

Halliday, A.N., 2008. A young Moon-forming giant 70–110 million years accompanied by late-stage mixing, core formation and degassing of the Earth. Philos. Trans. R. Soc. 366, 4163–4181.

Harrison, T.M., Schmitt, A.K., McCulloch, M.T., Lovera, O.M., 2008. Early ($\geqslant$4.5 Ga) formation of the terrestrial crust: Lu–Hf, $\delta^{18}O$, and Ti thermometry results for Hadean zircons. Earth Planet. Sci. Lett. 268, 476–486.

Hess, P.C., Parmentier, E.M., 1995. A model for the thermal and chemical evolution of the Moon's interior: implications for the onset of mare volcanism. Earth Planet. Sci. Lett. 134, 501–514.

Hurwitz, D.M., Kring, D.A., 2013. Composition and structure of the South Pole Aitken Basin impact melt sheet. In: 44th Lunar Planetary Science Conference #2224.

Jacobson, S.A., Morbidelli, A., Rayond, S.N., O'Brien, D.P., Walsh, K.J., Rubie, D.C., 2014. Highly siderophile elements in Earth's mantle as a clock for the Moon-forming impact. Nature 508, 84–87.

Kleine, T., Palme, H., Mezger, K., Halliday, A., 2005. Hf–W chronometry of lunar metals and the age and early differentiation of the Moon. Science 310, 1671.

Kleine, T., Touboul, M., Bourdon, B., Nimmo, F., Mezger, K., Palme, H., Jacobsen, S.B., Yin, Q.-Z., Halliday, A.N., 2009. Hf-W chronology of the accretion and early evolution of asteroids and terrestrial planets. Geochim. Cosmochim. Acta 73, 5150–5188.

Kleine, T., Burkhardt, C., Spring, P., 2013. Chondritic Sm/Nd in terrestrial planets and the origin of nucleosynthetic ^{142}Nd variations. In: 44th Lunar and Planetary Science Conference #3020.

Kinoshita, N., Paul, M., Kashiv, Y., Collon, P., Deibel, C.M., DiGiovine, B., Greene, J.P., Henderson, D.J., Jiang, C.L., Marley, S.T., Nakanishi, T., Pardo, R.C., Rehm, K.E., Robertson, D., Scott, R., Schmitt, C., Tang, X.D., Vondrasek, R., Yokoyama, A., 2012. A shorter ^{146}Sm half-life measured and implications for ^{146}Sm–^{142}Nd chronology in the solar system. Science 335, 1614–1617.

Lingenfelter, R.E., Canfield, E.H., Hampel, V.E., 1972. The lunar neutron flux revisited. Earth Planet. Sci. Lett. 16, 355–369.

Loper, D.E., Werner, C.L., 2002. On lunar asymmetries 1. Tilted convection and crustal asymmetry. J. Geophys. Res. 107, 13-1–13-7.

Lucey, P., Korotev, R.L., Gillis, J.J., Taylor, L.A., Lawrence, D., Campbell, B.A., Elphic, R., Feldman, B., Hood, L.L., Hunten, D., Mendillo, M., Noble, S., Papike, J.J., Reedy, R.C., Lawson, S., Prettyman, T., Gasnault, O., Maurice, S., 2006. Understanding the lunar surface and Space–Moon interactions *in* new views of the Moon. Rev. Mineral. Geochem. 60, 83–219.

Lugmair, G.W., Carlson, R.W., 1978. The Sm–Nd history of KREEP. In: Proceedings of the Ninth Lunar Planetary Sci. Lunar Planetary Institute, Houston, pp. 689–704.

Marks, N., Borg, L., Gaffney, A., Shearer, C., Burger, P., 2014. Additional evidence for young ferroan anorthositic magmatism on the Moon from Sm–Nd isotopic measurements of 60016 clast 3A. In: 45th Lunar and Planetary Science Conference #1129.

Meyer, C., 2009. Lunar sample compendium. http://curator.jsc.nasa.gov/lunar/compendium.cfm.

Meyer, J., Elkins Tanton, L.T., Wisdom, J., 2010. Coupled thermal-orbital evolution of the early Moon. Icarus 208, 1–10.

Morbidelli, A., Marchi, S., Bottke, W.F., Kring, D.A., 2012. A sawtooth-like timeline for the first billion years of lunar bombardment. Earth Planet. Sci. Lett. 355–356, 144–151.

Murphy, D.T., Brandon, A.D., Debaille, V., Burgess, R., Ballentine, C., 2010. In search of a hidden long- term isolate sub-chondritic $^{142}Nd/^{143}Nd$ reservoir in the deep mantle: implications for the Nd isotope systematics of the Earth. Geochim. Cosmochim. Acta 74, 738–750.

Münker, C., 2010. A high field strength element perspective on early lunar differentiation. Geochim. Cosmochim. Acta 74, 7340–7361.

Neal, C.R., Hacker, M.D., Snyder, G.A., Taylor, L.A., Liu, Y.-G., Schmitt, R.A., 1994. Basalt generation at the Apollo 12 sites, Part 2: source heterogeneity, multiple melts and crustal contamination. Meteoritics 29, 349–361.

Nemchin, A.A., Pidgeon, R.T., Whitehouse, M.J., Vaughn, J.P., Meyer, C., 2008. SIMS U–Pb study of zircon from Apollo 14 and 17 breccias: implications for the evolution of lunar KREEP. Geochim. Cosmochim. Acta 72, 668–689.

Nemchin, A., Timms, N., Pidgeon, R., Geisler, Reddy, S., Meyer, C., 2009. Timing of crystallization of the lunar magma ocean constrained by the oldest zircon. Nat. Geosci. 2, 133–136.

Norman, M.D., Borg, L.E., Nyquist, L.E., Bogard, D.D., 2003. Chronology, geochemistry, and petrology of a ferroan noritic anorthosite clast from Descartes breccia 67215: clues to the age, origin, structure, and impact history of the lunar crust. Meteorit. Planet. Sci. 38, 645–661.

Nyquist, L.E., Shih, C.-Y., 1992. The isotopic record of lunar volcanism. Geochim. Cosmochim. Acta 56, 2213–2234.

Nyquist, L.E., Bansal, B.M., Wooden, J.L., Wiesmann, H., 1977. Sr-isotopic constraints on the petrogenesis of Apollo 12 mare basalts. In: Proc. Lunar. Sco. Conf. 8th, pp. 1383–1415.

Nyquist, L.E., Shih, C.-Y., Wooden, J.L., Bansal, B.M., Wiesmann, H., 1979. The Sr and Nd isotopic record of Apollo 12 basalts: implications for lunar geochemical evolution. In: Proc. Lunar. Planet. Sci. Conf. 10th, pp. 77–114.

Nyquist, L.E., Wiesmann, H., Bansai, B., Shih, C.-Y., Keith, J.E., Harper, C.L., 1995. ^{146}Sm–^{142}Nd formation interval for the lunar mantle. Geochim. Cosmochim. Acta 59, 2817–2837.

Nyquist, et al., 2006. Feldspathic clasts in Yamato-86032: remnants of the lunar crust with implications for its formation and impact history. Geochim. Cosmochim. Acta 70, 5990–6015.

O'Neill, St.H.C., Palme, H., 2008. Collisional erosion and the non-chondritic composition of the terrestrial planets. Philos. Trans. R. Soc. 366, 4205–4238.

Ozima, M., Podosek, F.A., 1999. Formation age of Earth from $^{129}I/^{127}I$ and $^{244}Pu/^{238}U$ systematics and the missing Xe. J. Geophys. Res. 104, 25493–25499.

Papike, J.J., Hodges, F.N., Bence, A.E., 1976. Mare basalts: crystal chemistry, mineralogy and petrology. Rev. Geophys. Space Phys. 14, 475–540.

Rankenburg, K., Brandon, A.D., Neal, C.R., 2006. Neodymium isotope evidence for a chrondritic composition of the Moon. Science 312, 1369–1372.

Rehkämper, M., Gärtner, M., Galer, S.J.G., Goldstein, S.L., 1996. Separation of Ce from other rare- earth elements with application to Sm–Nd and La–Ce chronometry. Chem. Geol. 129, 201–208.

Ryder, G., 1991. Lunar ferroan anorthosites and mare basalt sources: the mixed connection. Geophys. Res. Lett. 18, 2065–2068.

Shearer, C., Hess, P.C., Wieczorek, M.A., Pritchard, M.E., Parmentier, E.M., Borg, L.E., Longhi, J., Elkins-Tanton, L.T., Neal, C.R., Antonenko, I., Canup, R., Halliday, A.N., Grove, T.L., Hager, B.H., Lee, D.-C., Wiechert, 2006. Thermal and magmatic evolution of the moon in new views of the Moon. Rev. Mineral. Geochem. 60, 365–518.

Shih, C.-Y., Nyquist, L.E., Reese, Y., Yamaguchi, A., 2005. Rb–Sr and Sm–Nd isotopic studies of Lunar Highland Meteorite Y86032 and Lunar Ferroan Anorthosites 60025 and 67075. In: Proc. Lunar. Planet. Sci. Conf. 36th, #1433.

Snyder, G.A., Taylor, L.A., Neal, C.R., 1992. A chemical model for generating the sources of mare basalts: combined equilibrium and fractional crystallization of the lunar magmasphere. Geochim. Cosmochim. Acta 56, 3809–3823.

Snyder, G.A., Neal, C.R., Taylor, L.A., Halliday, A.N., 1997. Anatexis of lunar cumulate mantle in time and space: clues from trace-element, strontium and neodymium isotopic chemistry of parental Apollo 12 basalts. Geochim. Cosmochim. Acta 61, 2731–2747.

Solomon, S.C., Longhi, J., 1977. Magma Oceanography: 1. Thermal evolution. In: Proc. Lunar. Planet. Sci. Conf. 8th, pp. 583–599.

Sprung, P., Kleine, T., Scherer, E.E., 2013. Isotopic evidence for chondritic Lu/Hf and Sm/Nd of the Moon. Earth Planet. Sci. Lett. 380, 77–87.

Taylor, S.R., 1973. Chemical evidence for lunar melting and differentiation. Nature 245, 203–205.

Taylor, S.R., Jakes, P., 1974. The geochemical evolution of the moon. In: Proceedings of the Fifth Lunar Conference. Geochim. Cosmochim. Acta Supplement 5, 1287–1305.

Taylor, D.J., McKeegan, K.D., Harrison, T.M., 2009. Lu–Hf zircon evidence for rapid lunar differentiation. Earth Planet. Sci. Lett. 279, 157–164.
Tera, F., Wasserburg, G.J., 1974. U–Th–Pb systematics on lunar rocks and inferences about lunar evolution and the age of the Moon. In: Proceedings of the Fifth Lunar Conference. Geochim. Cosmochim. Acta Supplement 5, 1571–1599.
Touboul, M., Kleine, T., Bourdon, B., Palme, H., Wieler, R., 2007. Late formation and prolonged differentiation of the Moon inferred from W isotopes in lunar metals. Nature 450, 1206–1209.
Trinquier, A., Elliot, T., Ulfbeck, D., Coath, C., Krot, A., Bizarro, M., 2009. Origin of nucleosynthetic isotope heterogeneity in the solar protoplanetary disk. Science 324, 374–376.
Valley, et al., 2014. Hadean age for a post-magma ocean zircon confirmed by atom probe tomography. Nat. Geosci. 7, 219–223.
Wasserburg, G.J., Jacobsen, S.B., DePaolo, D.J., McCulloch, M.T., Wen, T., 1981. Precise determination of Sm/Nd ratios, Sm and Nd isotopic abundances in standard solutions. Geochim. Cosmochim. Acta 45, 2311–2323.